

# cryoEM-Guided Development of Antibiotics for Drug-Resistant Bacteria

Matthew J. Belousoff,<sup>[a]</sup> Hari Venugopal,<sup>[b]</sup> Alexander Wright,<sup>[c]</sup> Samuel Seoner,<sup>[c]</sup> Isabella Stuart,<sup>[a]</sup> Chris Stubenrauch,<sup>[a]</sup> Rebecca S. Bamert,<sup>[a]</sup> David W. Lupton,<sup>\*,[c]</sup> and Trevor Lithgow<sup>\*,[a]</sup>

While the ribosome is a common target for antibiotics, challenges with crystallography can impede the development of new bioactives using structure-based drug design approaches. In this study we exploit common structural features present in linezolid-resistant forms of both methicillin-resistant *Staphylococcus aureus* (MRSA) and vancomycin-resistant *Enterococcus* (VRE) to redesign the antibiotic. Enabled by rapid and facile cryoEM structures, this process has identified (S)-2,2-dichloro-N-((3-(3-fluoro-4-morpholinophenyl)-2-oxooxazolidin-5-yl)methyl)acetamide (LZD-5) and (S)-2-chloro-N-((3-(3-fluoro-4-morpholinophenyl)-2-oxooxazolidin-5-yl)methyl) acetamide (LZD-6), which inhibit the ribosomal function and growth of linezolid-resistant MRSA and VRE. The strategy discussed highlights the potential for cryoEM to facilitate the development of novel bioactive materials.

Combating antimicrobial resistance requires multiple therapeutic strategies, including the discovery of new molecular scaffolds, re-engineering and repurposing of existing drugs, in addition to improvements in antimicrobial stewardship.<sup>[1]</sup> The discovery of small molecules with antimicrobial activity can be facilitated by structure-based drug design (SBDD) strategies.<sup>[2]</sup> Approaches of this type exploit structural information, obtained using various biochemical assays, to drive the drug design process. Although a number of techniques are employed in SBDD, the field remains heavily reliant on X-ray<sup>[3]</sup> and NMR-based analysis,<sup>[4]</sup> techniques with orthogonal advantages with regard to resolution, throughput, and analysis cost. With the emergence of high-resolution cryoEM as a powerful tool for determining structural information, its ability to be applied in SBDD, particularly when examining biomolecules poorly suited to X-ray analysis, has been discussed extensively.<sup>[5]</sup> In ad-

dition to reaching resolution targets that allow unambiguous placement of small molecules, cryoEM is a solution-phase technique which may prove advantageous. Although cryoEM-guided design of novel ligands is underdeveloped, the interactions of known drugs with their targets have been examined with the *Plasmodium* 20S proteasome,<sup>[6]</sup> the GPCR family,<sup>[7]</sup> pathogenic ribosomes,<sup>[8]</sup> receptor-bound insulin,<sup>[9]</sup> and important HIV viral entry proteins,<sup>[10]</sup> to name a few examples. In 2017, Scheres, Baum, and co-workers exploited cryoEM to elucidate the mode of action that mefloquine uses to inhibit the *Plasmodium falciparum* ribosome, and then used this insight to develop a next-generation molecule with enhanced antiparasitic activity.<sup>[11]</sup> As part of our studies into mechanisms of antibiotic resistance, we examined one of the escape routes that *Staphylococcus aureus* uses to develop resistance to the ribosomal-interfering antibiotic, linezolid.<sup>[8a]</sup> These studies, and those of others,<sup>[12]</sup> show that disparate mutations result in a common structural rearrangement that lowers the affinity of linezolid binding at the peptidyl transferase center (PTC), suggesting that in order to preserve its enzymatic activity, the ribosome is not infinitely malleable.<sup>[8a, 12a, 13]</sup> Taking advantage of these common structural changes in linezolid-resistant (Lin<sup>R</sup>) strains, we postulated that simple modification of an amide group in linezolid should reintroduce binding to the altered A-site. Herein we report studies on this topic which have exploited cryoEM to guide the development of new linezolid analogues that target Lin<sup>R</sup> strains of MRSA and VRE. Central to this work was a cryoEM workflow that allowed rapid delivery of high-resolution structural information. This strategy should have potential value in many areas of SBDD.

The bacterial ribosome is a common target for drug development, with over 40% of antibiotics in clinical use targeting its activity in protein synthesis.<sup>[14]</sup> The first-in-class oxazolidinone antibiotic<sup>[15]</sup> linezolid is one of the most recently introduced drugs. Linezolid is widely used for the treatment of infections caused by bacterial resistance to antibiotics such as methicillin and vancomycin, particularly MRSA and VRE.<sup>[13a, 16]</sup> Linezolid binds to rRNA in the A-site of the peptidyl transferase center of the ribosome (SI Figure S1), and inhibits protein synthesis by sterically blocking recruitment of aminoacyl-tRNA. As a first step in re-engineering a form of linezolid that could bind and inhibit the altered A-site in Lin<sup>R</sup> strains, we examined the characteristics of the compacted drug-binding site in the Lin<sup>R</sup> ribosome. A large conformational change of the rRNA residues U<sup>2506</sup> and G<sup>2505</sup> (*E. coli* numbering used throughout) was observed, which in turn remodels the linezolid-binding pocket

[a] Dr. M. J. Belousoff, I. Stuart, Dr. C. Stubenrauch, R. S. Bamert, Prof. T. Lithgow  
Infection and Immunity Program, Department of Microbiology, Monash University, Clayton 3800 (Australia)  
E-mail: trevor.lithgow@monash.edu

[b] H. Venugopal  
Ramaciotti Centre for Electron Microscopy, Monash University, Clayton 3800 (Australia)

[c] A. Wright, S. Seoner, Prof. D. W. Lupton  
School of Chemistry, Monash University, Clayton 3800 (Australia)  
E-mail: david.lupton@monash.edu

 Supporting information and the ORCID identification number(s) for the author(s) of this article can be found under:  
<https://doi.org/10.1002/cmdc.201900042>

(Figure 1 a, SI Figure S2a). Comparative analysis of these various mutant ribosomes revealed a highly similar conformation in most of the rRNA residues, raising the prospect that an induced-fit mode of binding may be possible in the peptidyl transferase pocket. The largest conformational change in the Lin<sup>R</sup> ribosome structure impacted the position of the oxazolidinone heterocycle (SI Figure S1 a). In a linezolid:70S ribosome complex, the amide carbonyl group points toward G<sup>2447</sup>, making a putative hydrogen bond with A<sup>2451</sup> (SI Figure S2 b). A

rational analysis of the structural coordinates for the Lin<sup>R</sup> ribosome (SI Figure S2) revealed binding opportunities for an amide at the 5-position if it were redirected toward A<sup>2503</sup>, where a larger pocket is present that could potentially accommodate a bulkier amide than the acyl group present in linezolid (SI Figure S2). If such reorientation could be achieved, then linezolid-based analogues should prove capable of evading contraction-based drug resistance. To address this hypothesis, a selection of amides at the 5-position of linezolid starting with the common amine (S)-5-(aminomethyl)-3-(3-fluoro-4-morpholinophenyl)oxazolidone-2 (**2**) itself,<sup>[17]</sup> were prepared (Figure 1 b).

While the compounds displayed in Figure 1 would not necessarily be viable clinical antibiotics due to undesirable pharmacokinetics (solubility) and pharmacodynamics (potential toxicity; LZD-7 being a potential Michael acceptor and the halogenated compounds containing labile leaving groups), they were selected to examine the viability of cryoEM as a tool of value for targeting ligand biomolecule interactions.

Screening the compounds in a minimal inhibitory concentration (MIC) assay demonstrated that the compounds were active as antibiotics in vitro (Table 1). The chloro (LZD-6) and

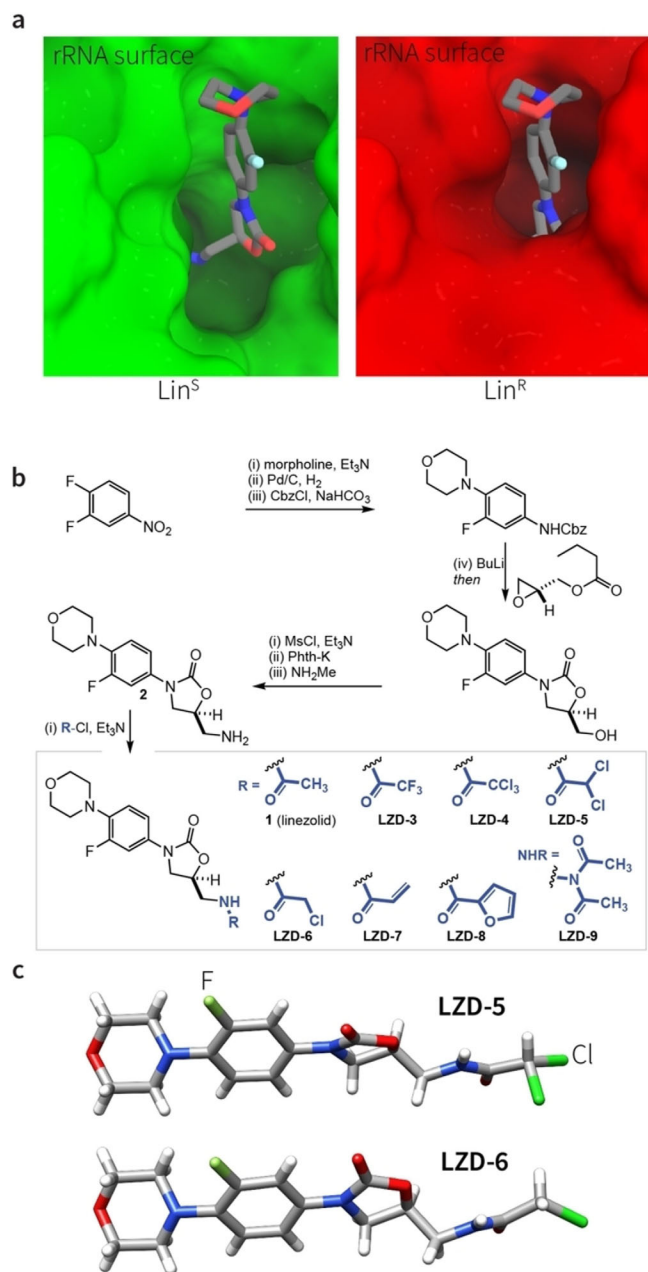


**Figure 1.** a) View of the drug-binding pocket from the cryoEM structures of the 70S ribosomes from Lin<sup>S</sup> (PDB ID: 5TCU and EMDB EMD-8402; left panel) and Lin<sup>R</sup> (PDB ID: 5T7V and EMDB EMD-8369; right panel) MRSA strains. Overlaid is the binding position of linezolid. Green and red surfaces are the solvent-accessible surface of the rRNA about the site of linezolid binding. b) Synthetic scheme used to synthesize LZD-3–9.<sup>[17]</sup> c) Stick representation of the X-ray crystal structures of LZD-5 and LZD-6.

**Table 1.** Minimum inhibitory concentration for antibiotics against relevant bacterial species: *Staphylococcus aureus*, *Staphylococcus capitis*, *Staphylococcus epidermidis*, and vancomycin-resistant *Enterococcus* (VRE, ATCC700221).

Compound	MIC [ $\mu\text{g mL}^{-1}$ ] <sup>[a]</sup>				
	<i>S. aur.</i>	MRSA (Lin <sup>R</sup> )	<i>S. cap.</i>	<i>S. epi.</i>	VRE
linezolid	0.5	2	0.5	0.25	1
LZD-3	1	4	1	1	2
LZD-4	2	4	1	1	2
LZD-5	0.5	1	0.25	0.25	0.5
LZD-6	0.25	1	0.25	0.13	0.25
LZD-7	1	2	1	0.5	1
LZD-8	2	8	2	2	4
LZD-9	4	16	2	2	4

[a] MIC assays were carried out according to CLSI protocols.<sup>[18]</sup>

dichloro (LZD-5) derivatives were the most active in inhibiting growth of Lin<sup>R</sup> MRSA. These compounds bind to both the linezolid-sensitive (Lin<sup>S</sup>) and Lin<sup>R</sup> states of the drug-binding pocket on the ribosome, as they inhibit both Lin<sup>S</sup> and Lin<sup>R</sup> strains of *S. aureus* (Table 1). X-ray crystallographic analysis of LZD-5 and LZD-6 (Figure 1 c, SI Figure S3) showed a similar overall structure, with both crystallising in the same space group with very similar unit cells (SI Table S1). Both showed a “linear” topology with two molecules exhibiting a head-to-tail van der Waals interaction, which formed the basis of the asymmetric unit of the crystal lattice. The 2-oxazolidone moiety of both LZD-5 and LZD-6, lying in the same plane as the fluorinated aromatic ring (although LZD-5 showed a greater offset between the plane of the aromatic ring and the 2-oxazolidone ring which was 30° compared to 8° in LZD-6). None of the other derivatives showed improved activity, while some were significantly worse. For example, the imide derivative LZD-9 showed relatively poor MIC values for all bacterial strains (Table 1).

To assess whether the improved potency of LZD-5 and LZD-6 was driven by more effective inhibition of ribosomal activity, we assayed the compounds in a cell-free translation system. In this system, synthesis of firefly luciferase is used to monitor ribosomal activity using a luminescence readout. LZD-5 and LZD-6 were more effective at inhibiting protein synthesis by the ribosome than was the parent compound linezolid (Table 2).

Compound	IC <sub>50</sub> [μM] <sup>[a]</sup>
linezolid	3.8 ± 0.3
LZD-3	6 ± 1
LZD-4	3.9 ± 0.7
LZD-5	2.6 ± 0.2
LZD-6	2.6 ± 0.5
LZD-7	5 ± 1
LZD-8	> 40
LZD-9	> 30

[a] IC<sub>50</sub> plots are provided in Supporting Information Figure S8; values are the mean ± SEM (n = 3).

To determine if the improved activity was due to the foreshadowed conformational changes, single-particle cryoEM data was collected yielding refined maps for LZD-5:70S and LZD-6:70S to a global resolution of 3.1 and 2.8 Å, respectively (SI Figure S4a). As the molecules of interest bind in the 50S ribosomal subunit, Euler angle refinement was focused on the 50S subunit. This allowed well-resolved maps around the peptidyl transferase center, with the local resolutions around the area of interest both being < 2.9 Å (SI Figure S4b,c). Given reports that use of the Volta Phase Plate (VPP) may lead to more facile visualisation of small bound ligands due to its higher contrast micrographs (SI Figure S5a),<sup>[20]</sup> the LZD-5:70S structure was collected using a VPP, while the LZD-6:70S was collected using a standard varied defocus strategy. Both maps are strikingly similar, with the atomic structures superimposable (SI Figure S3). Using the VPP collection we were able to collect high-quality data (SI Figure S5b,c), which resulted in similar resolution (SI Figure S2a,b) but with significantly fewer micrographs (SI Table S2). By periodic movement of the VPP, we were able to keep the phase shift within suitable boundaries (SI Figure S5d,e) leading to high-quality reconstructions (SI Figure S5f) and similar map quality (SI Figure S6a) to the varied defocus collection. This means a substantial decrease in valuable microscope time to achieve equally high-quality and interpretable data for unambiguous drug placement in the ribosome.

The density map around LZD-6 was interpretable at 2.8 Å resolution, and the position and stereochemistry of the molecule could be placed unambiguously (Figure 2a). LZD-6 adopts a similar binding position to that of linezolid (Figure 2b); however, the 2-chloroacyl group is now directed toward rRNA residue A<sup>2503</sup> and the 2-oxazolidone ring is in a slightly different orientation to maximise hydrophobic interactions with U<sup>2504</sup>

and accommodate the different acyl group position (Figure 2c). Relative to the crystal structure of LZD-6 alone, which adopts a linear topology, the acyl tail rotates around the amide bond to form more favorable interactions with the surrounding rRNA when in complex with the ribosome. This different mode of binding shows that there is a degree of flexibility in the binding of the oxazolidinone pharmacophore to the PTC, and that the representative linezolid binding<sup>[19]</sup> is not the only rigid option for this family of antibiotics.

In the ribosome, LZD-6 is assisted by additional interactions with surrounding rRNA residues (Figure 2d). The 2-chloroacyl group forms a hydrogen bond with the ribose of A<sup>2503</sup>, while a hydrophobic interaction with the purine of A<sup>2503</sup>, and a π-π interaction with the purine of G<sup>2061</sup> are also gained (Figure 2e). These interactions allow the 2-oxazolidone ring to form a favorable hydrophobic interaction with pyrimidine of U<sup>2504</sup>. All other interactions with the morpholine and the fluorophenyl ring are similar to linezolid, except that the morpholine ring in LZD-5 and LZD-6 forms a hydrogen bond with the ribose of A<sup>2451</sup>. These observations also provide a potential explanation for why tedizolid, a new oxazolidinone antibiotic, effectively binds the ribosome without having a morpholine, as it might promote an induced fit at a similar location to interact with A<sup>2451</sup> via a hydrogen bond between tedizolid's pyridine ring and the ribose sugar.<sup>[21]</sup>

While LZD-6 had two-fold greater ability to inhibit bacterial growth, we set out to examine if the decreased MIC activity correlated with any decrease in the acquisition of drug resistance. The evolution of resistance toward LZD-6 by *S. aureus* was determined by serially passaging *S. aureus* through broth containing various concentrations of LZD-6. After 16 days of serial passaging on 0.5 μg mL<sup>-1</sup> LZD-6, a spontaneous mutant was isolated. This mutant was cultured and shown to be drug-resistant *S. aureus* by serial broth microdilution, yielding a MIC value of 2 μg mL<sup>-1</sup>. The rate at which the drug-resistant *S. aureus* evolved is ≈ 1 cell per < 10<sup>8</sup> generations, which is more rapid than the observed rate of ≈ 1 cell per < 10<sup>10</sup> generations for the parent compound, linezolid. However, it was found that while the MIC value of the resistance mutant was four-fold greater than the starting strain, the LZD-6 resistance phenotype came with a mild fitness cost, as evidenced by a slower growth phenotype (SI Figure S7a,b). This fitness versus resistance cost had an even more profound effect when we generated resistance mutants by long-period static growth at sub-MIC concentrations of LZD-6 (SI Figure S7c,d).

Medicinal chemistry approaches to developing antibiotics, particularly targeting the ribosome, can be hampered by challenges gaining structural information from which to design novel compounds. Exploiting knowledge of structural changes in the ribosomal drug-binding pocket that gives rise to linezolid resistance in MRSA, we have designed analogues of linezolid that overcome these changes, thereby binding and inhibiting the Lin<sup>R</sup> ribosome. There is reason to believe that in vivo, the evolution of resistance to LZD-5 and LZD-6 will be more challenging to bacteria, given that these compounds bind through an induced fit into both states (i.e., Lin<sup>S</sup> and Lin<sup>R</sup>) of the drug-binding pocket and given that the active site of the ribosome

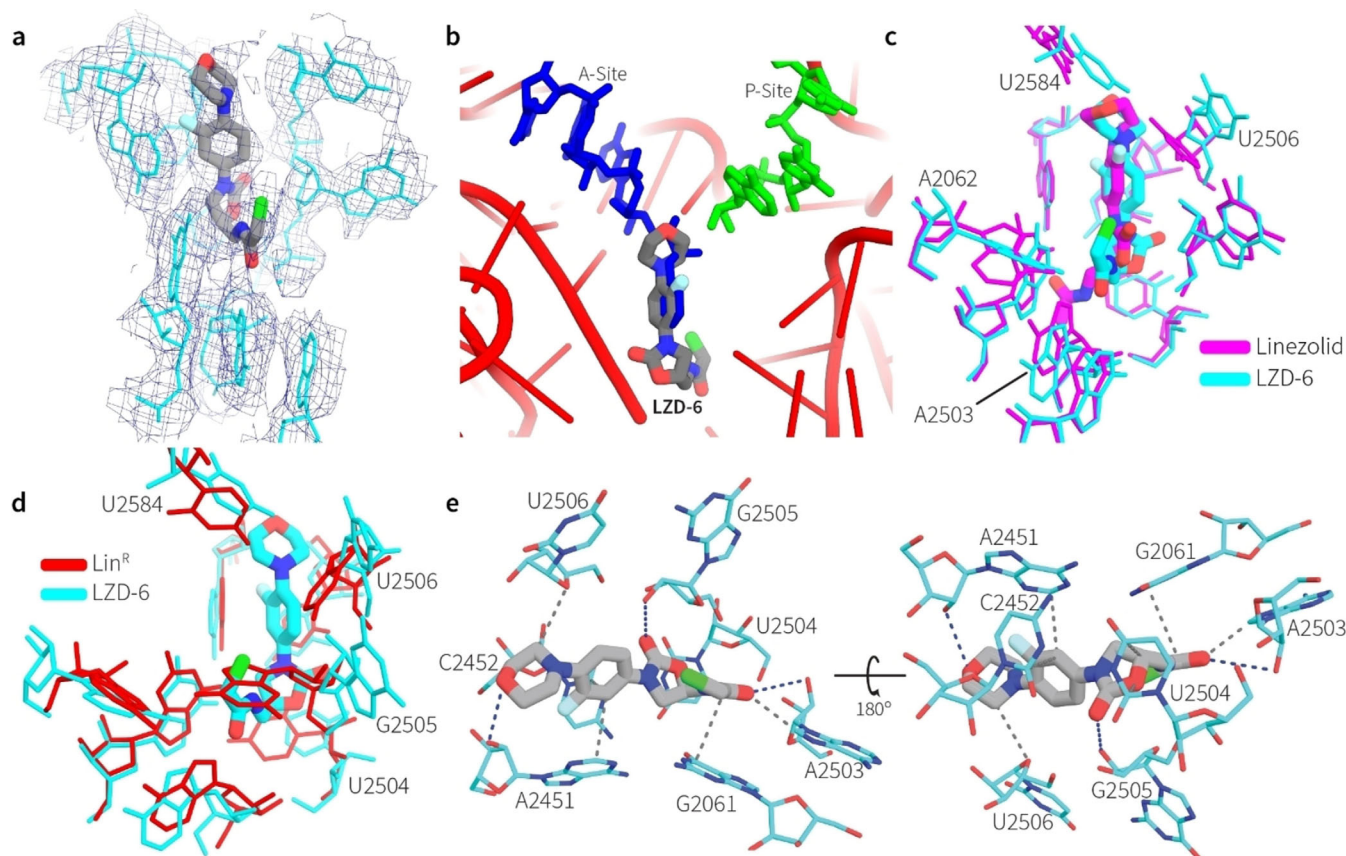


**Figure 2.** a) Diagrammatic representation of the cryoEM structure of the peptidyl transferase center in the 50S ribosomal subunit from MRSA with LZD-6 bound at the peptidyl transferase center,<sup>[19]</sup> highlighting how LZD-6 would inhibit protein synthesis by blocking binding of incoming tRNA into the A-site. Overlaid are the positions of the 3' end of the tRNAs in the A-site and P-site (blue and green, respectively). b) CryoEM density map drawn at  $4\sigma$  around the binding site of LZD-6 in the A-site of the peptidyl transferase center (PTC). Stick representations show the rRNA residues; thicker sticks show the oxazolidinone molecule. c) Cartoon representation of the structural superposition of the binding region of the LZD-6:70S complex (cyan) and the linezolid:70S complex (magenta) structure (PDB ID: 4WFA).<sup>[19]</sup> d) Cartoon representation of the structural superposition of the binding region of both the LZD-6:70S complex (cyan) and the same region of the Lin<sup>R</sup> ribosome structure (red) from MRSA (PDB ID: 5T7V).<sup>[8a]</sup> e) Enlargement of the binding site of LZD-6 (grey and CPK coloring) in the drug-binding pocket, showing in dotted lines interactions with surrounding rRNA residues (blue: hydrogen bond interactions; grey: van der Waals/ $\pi$ - $\pi$  interactions); left and right are  $180^\circ$  rotations about the viewing plane.

where the compounds bind is not infinitely malleable and that there is an observable growth fitness cost that coincides with resistance. Structural analysis of the modified drug bound to the ribosome showed how these modified structures induced a fit to the ribosome through additional interactions with rRNA residues in the binding pocket. This work showcases the use of cryoEM as a framework for the rational design of new antibiotics. Although LZD-5 and 6 are unlikely to display drug-like features, ongoing work in our laboratories is focused on the use of cryoEM to provide facile access to structural information of value to the pursuit of novel antibiotics.

## Experimental Section

Detailed method descriptions are available in the Supporting Information. All figures were generated with either PyMOL or UCSF Chimera. The atomic structures have been deposited in the RCSB Protein Data Bank with accession codes 6DDD for LZD-5-MRSA50S and 6DDG for LZD-6-MRSA50S. The cryoEM density maps were deposited in the Electron Microscopy Data Bank under accession

codes EMD-7867 for LZD-5-MRSA50S and EMD-7870 for LZD-6-MRSA50S.

## Acknowledgements

We acknowledge the support staff and facilities at the Monash Ramaciotti Centre for Cryo-Electron Microscopy. We thank Georg Ramm for Titan Krios support, Anton Peleg for providing clinical isolates of MRSA and VRE, and Ana Traven and Jamie Rossjohn for comments on the manuscript. We acknowledge the NVIDIA Corporation for donating GPUs to aid with calculations used in this research. This work was supported by the Multi-modal Australian ScienceS Imaging and Visualisation Environment (MAS-SIVE) ([www.massive.org.au](http://www.massive.org.au)). The work was funded by the National Health & Medical Research Council of Australia (Program Grant 1092262 to T.L.) and the Australia Research Council (DP 170103567 to D.W.L.). The funders had no role in study design, data collection and interpretation, or the decision to submit the work for publication.

## Conflict of interest

The authors declare no conflict of interest.

**Keywords:** antibiotic resistance · cryoEM · linezolid · structure-based drug design

- [1] a) D. Brown, *Nat. Rev. Drug Discovery* **2015**, *14*, 821–832; b) A. Du Toit, *Nat. Rev. Microbiol.* **2016**, *14*, 725; c) V. W. Soo, B. W. Kwan, H. Quezada, I. Castillo-Juarez, B. Perez-Eretza, S. J. Garcia-Contreras, M. Martinez-Vazquez, T. K. Wood, R. Garcia-Contreras, *Curr. Top. Med. Chem.* **2017**, *17*, 1157–1176.
- [2] K. J. Simmons, I. Chopra, C. W. Fishwick, *Nat. Rev. Microbiol.* **2010**, *8*, 501–510.
- [3] a) T. L. Blundell, H. Jhoti, C. Abell, *Nat. Rev. Drug Discovery* **2002**, *1*, 45–54; b) A. C. Anderson, *Chem. Biol.* **2003**, *10*, 787–797.
- [4] a) D. A. Erlanson, S. W. Fesik, R. E. Hubbard, W. Jahnke, H. Jhoti, *Nat. Rev. Drug Discovery* **2016**, *15*, 605–619; b) D. C. Rees, M. Congreve, C. W. Murray, R. Carr, *Nat. Rev. Drug Discovery* **2004**, *3*, 660–672.
- [5] a) G. Scapin, C. S. Potter, B. Carragher, *Cell Chem. Biol.* **2018**, *25*, 1318–1325; b) A. Merk, A. Bartesaghi, S. Banerjee, V. Falconieri, P. Rao, M. I. Davis, R. Pragani, M. B. Boxer, L. A. Earl, J. L. S. Milne, S. Subramaniam, *Cell* **2016**, *165*, 1698–1707; c) X. C. Bai, G. McMullan, S. H. Scheres, *Trends Biochem. Sci.* **2015**, *40*, 49–57; d) F. Merino, S. Raunser, *Angew. Chem. Int. Ed.* **2017**, *56*, 2846–2860; *Angew. Chem.* **2017**, *129*, 2890–2905.
- [6] H. Li, M. Bogyo, P. C. da Fonseca, *FEBS J.* **2016**, *283*, 4238–4243.
- [7] Y. L. Liang, M. Khoshouei, M. Radjainia, Y. Zhang, A. Glukhova, J. Tarasch, D. M. Thal, S. G. B. Furness, G. Christopoulos, T. Coudrat, R. Danev, W. Baumeister, L. J. Miller, A. Christopoulos, B. K. Kobilka, D. Wootten, G. Skiniotis, P. M. Sexton, *Nature* **2017**, *546*, 118–123.
- [8] a) M. J. Belousoff, Z. Eyal, M. Radjainia, T. Ahmed, R. S. Bamert, D. Matzov, A. Bashan, E. Zimmerman, S. Mishra, D. Cameron, H. Elmlund, A. Y. Peleg, S. Bhushan, T. Lithgow, A. Yonath, *MBio* **2017**, *8*, e00395-17; b) N. Fischer, P. Neumann, A. L. Konevega, L. V. Bock, R. Ficner, M. V. Rodnina, H. Stark, *Nature* **2015**, *520*, 567–570.
- [9] G. Scapin, V. P. Dandey, Z. Zhang, W. Prosiise, A. Hruza, T. Kelly, T. Mayhood, C. Strickland, C. S. Potter, B. Carragher, *Nature* **2018**, *556*, 122–125.
- [10] D. Lyumkis, J. P. Julien, N. de Val, A. Cupo, C. S. Potter, P. J. Klasse, D. R. Burton, R. W. Sanders, J. P. Moore, B. Carragher, I. A. Wilson, A. B. Ward, *Science* **2013**, *342*, 1484–1490.
- [11] W. Wong, X. C. Bai, B. E. Sleebs, T. Triglia, A. Brown, J. K. Thompson, K. E. Jackson, E. Hanssen, D. S. Marapana, I. S. Fernandez, S. A. Ralph, A. F. Cowman, S. H. W. Scheres, J. Baum, *Nat. Microbiol.* **2017**, *2*, 17031.
- [12] a) K. S. Long, B. Vester, *Antimicrob. Agents Chemother.* **2012**, *56*, 603–612; b) J. B. Locke, M. Hilgers, K. J. Shaw, *Antimicrob. Agents Chemother.* **2009**, *53*, 5265–5274.
- [13] a) R. Bi, T. Qin, W. Fan, P. Ma, B. Gu, *J. Global Antimicrob. Resist.* **2017**, *13*, 11–19; b) T. A. Cidral, M. C. Carvalho, A. M. Figueiredo, M. C. de Melo, *APMIS* **2015**, *123*, 867–871; c) S. Tsiodras, H. S. Gold, G. Sakoulas, G. M. Eliopoulos, C. Wennersten, L. Venkataraman, R. C. Moellering, M. J. Ferraro, *Lancet* **2001**, *358*, 207–208.
- [14] a) J. Poehlsgaard, S. Douthwaite, *Nat. Rev. Microbiol.* **2005**, *3*, 870–881; b) D. N. Wilson, *Nat. Rev. Microbiol.* **2014**, *12*, 35–48; c) J. Lin, D. Zhou, T. A. Steitz, Y. S. Polikanov, M. G. Gagnon, *Annu. Rev. Biochem.* **2018**, *87*, 451–478.
- [15] K. J. Shaw, M. R. Barbachyn, *Ann. N. Y. Acad. Sci.* **2011**, *1241*, 48–70.
- [16] A. M. Bal, M. Z. David, J. Garau, T. Gottlieb, T. Mazzei, F. Scaglione, P. Tattevin, I. M. Gould, *J. Global Antimicrob. Resist.* **2017**, *10*, 295–303.
- [17] S. J. Brickner, D. K. Hutchinson, M. R. Barbachyn, P. R. Manninen, D. A. Ulanowicz, S. A. Garmon, K. C. Grega, S. K. Hendges, D. S. Toops, C. W. Ford, G. E. Zurenko, *J. Med. Chem.* **1996**, *39*, 673–679.
- [18] *Clinical and Laboratory Standards Institute (2015) Performance Standards for Antimicrobial Susceptibility Testing, 25th Informational Supplement*, CLSI Document M100-S25, Clinical and Laboratory Standards Institute, Wayne, PA (USA).
- [19] Z. Eyal, D. Matzov, M. Krupkin, I. Wekselman, S. Paukner, E. Zimmerman, H. Rozenberg, A. Bashan, A. Yonath, *Proc. Natl. Acad. Sci. USA* **2015**, *112*, E5805–E5814.
- [20] O. von Loeffelholz, G. Papai, R. Danev, A. G. Myasnikov, S. K. Natchiar, I. Hazemann, J. F. Menetret, B. P. Klaholz, *J. Struct. Biol.* **2018**, *202*, 191–199.
- [21] G. G. Zhanel, R. Love, H. Adam, A. Golden, S. Zelenitsky, F. Schweizer, B. Gorityala, P. R. Lagace-Wiens, E. Rubinstein, A. Walkty, A. S. Gin, M. Gil-mour, D. J. Hoban, J. P. Lynch III, J. A. Karlowsky, *Drugs* **2015**, *75*, 253–270.

Manuscript received: January 20, 2019

Accepted manuscript online: January 22, 2019

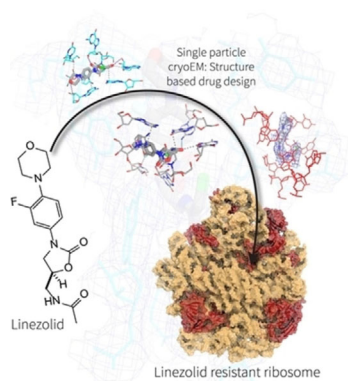
Version of record online: ■■■■■ 0000

## COMMUNICATIONS

M. J. Belousoff, H. Venugopal, A. Wright,  
S. Seoner, I. Stuart, C. Stubenrauch,  
R. S. Bamert, D. W. Lupton,\* T. Lithgow\*



### cryoEM-Guided Development of Antibiotics for Drug-Resistant Bacteria



**The bacterial ribosome** is a common target for antibiotics. However, it is a difficult drug target for structural study by conventional X-ray crystallography. We report the use of single-particle cryo-electron microscopy to aid in the structure-based drug design of new antibiotics based on the oxazolidinone, linezolid. We use this technique to show by a rational design approach that it is possible to synthesise new antibiotics with antibacterial activity against linezolid-resistant forms of both methicillin-resistant *Staphylococcus aureus* and vancomycin-resistant *Enterococcus*.